Biol. Cybern. 76, 163–171 (1997)

Biological Cybernetics

Human arm stiffness and equilibrium-point trajectory during multi-joint movement

Hiroaki Gomi [1], **Mitsuo Kawato** [2]

[1] Information Science Research Laboratory, NTT Basic Research Laboratories, Wakamiya 3-1, Morinosato, Atsugi, Kanagawa Prefecture, Japan
[2] ATR Human Information Processing Research Laboratories, Hikaridai 2-2, Seika-cho, Soraku-gun, Kyoto Prefecture, Japan

Received: 12 June 1996 / Accepted in revised form: 23 October 1996

Abstract. By using a newly designed high-performance manipulandum and a new estimation algorithm, we measured human multi-joint arm stiffness parameters during multi-joint point-to-point movements on a horizontal plane. This manipulandum allows us to apply a sufficient perturbation to subject's arm within a brief period during movement. Arm stiffness parameters were reliably estimated using a new algorithm, in which all unknown structural parameters could be estimated independent of arm posture (i.e., constant values under any arm posture). Arm stiffness during transverse movement was considerably greater than that during corresponding posture, but not during a longitudinal movement. Although the ratios of elbow, shoulder, and double-joint stiffness were varied in time, the orientation of stiffness ellipses during the movement did not change much. Equilibrium-point trajectories that were predicted from measured stiffness parameters and actual trajectories were slightly sinusoidally curved in Cartesian space and their velocity profiles were quite different from the velocity profiles of actual hand trajectories. This result contradicts the hypothesis that the brain does not take the dynamics into account in movement control depending on the neuromuscular servo mechanism; rather, it implies that the brain needs to acquire some internal models of controlled objects.

1 Introduction

Because joint torque of the musculoskeletal system for movement is generated by the imbalance between tensions of agonist and antagonist muscles which have inherently spring-like properties, stiffness during movement is an important factor in the study of the biological motion control mechanism. A joint's spring-like property can be varied by changing the activation levels of agonist and antagonist muscles. Based on these properties and neural feedback, which together determine global musculoskeletal behavior, several hypothetical mechanisms for arm movement have been proposed as a natural expansion from posture maintenance control (for review see McIntyre and Bizzi 1993). The 'equilibrium-point (EP) control hypothesis' is an influential hypothesis of a control mechanism based on the mechanical stability of viscoelastic properties supplied by the neuromuscular system. This hypothesis can be divided into two versions: the λ-model (Feldman 1966, 1986) in which spinal reflexes and reciprocal inhibition mechanisms are explicitly represented, and the α-model (Bizzi et al. 1984) in which the supraspinal nervous system rather than the spinal reflexes in the primary muscle-activating mechanism.

The assertions of the EP control hypothesis may be divided into the following three levels: (1) The spring-like properties of the neuromuscular system are utilized in movement control. (2) The brain uses an EP trajectory as descending motor commands to the spinal cord. (3) The EP trajectory can simply be planned; thus, the brain does not need to solve the dynamics problem (Bizzi et al. 1992; Feldman and Levin 1995).

Few researchers doubt that the spring-like properties of the neuromuscular system are of significant importance in maintaining stable posture (Carew 1985; Carew and Ghez 1985). The crucial question, however, is how far this system by itself suffices to generate movements. If the spring-like property is sufficiently strong with appropriate damping, even fast and smooth movements could be executed without complex computations, by relying heavily on it as the above third level of the EP control hypothesis asserts [see recent debate in 'Controversies in Neuroscience I: Movement Control', Behav Brain Sci 15 (1992); 'Modeling the Control of Upper Limb Movement', Mot Behav 25 (1993)].

In some studies of the EP control hypothesis, it was believed that EP trajectories can be relatively easily planned regardless of complex computations considering controlled object dynamics (Bizzi et al. 1992; Feldman

Correspondence to: H. Gomi (Fax: + 81-462-40-4721, e-mail: gomi@idea.brl.ntt.jp)

and Levin 1995). In other contexts, since the limb is expected to realize a trajectory which is similar to the EP trajectory (Flash 1987; McIntyre and Bizzi 1993), and because it is known that arm movements can be approximated with simple geometric curves (Kelso et al. 1979; Morasso 1981; Abend et al. 1982; Flash and Hogan 1985), it was hypothesized that the EP trajectory should be planned in a simple way.

On the other hand, several simulation studies (Hogan 1984; Flash 1987; Flanagan et al. 1993; Katayama and Kawato 1993; McIntyre and Bizzi 1993) conducted to investigate the above question revealed the critical importance of the magnitude of arm stiffness during movement. That is, if the arm stiffness during movement is high [e.g., the joint stiffness is 67.9 N m/rad for shoulder and 78.0 N m/rad for elbow on average in Flash (1987)], then the EP trajectory is similar to the actual one, and complex computation is thus not necessary. In contrast, if dynamic stiffness is low [e.g, 19.5 N m/rad for shoulder and 15 N m/rad for elbow in Katayama and Kawato (1993)], the two trajectories are very different.

The low stiffness and the remarkable differences between equilibrium and actual trajectories were experimentally demonstrated in single-joint fast movements (Latash and Gottlieb 1991; Bennett et al. 1992; Latash 1992a, b, 1994). In the single-joint movement, however, the inertial torque is linearly proportional to angular acceleration because of constant inertia; therefore, it may be possible to plan the EP trajectory by some simple scaling parameter depending on the movement speed (Latash 1992a). Thus, a single-joint study could be criticized on the grounds that, during multi-joint movement, the strategy could be different from that during single-joint movement because of variable inertia during movement. One of the potential merits of the EP control hypothesis is that the nonlinear dynamics of the controlled object do not need to be taken into account in movement control by the supraspinal nervous system (Bizzi et al. 1992). To verify the EP control hypothesis as a basic control mechanism for multi-joint arm movement, it is essential to measure the mechanical characteristics of the human arm during actual multi-joint movement. Although, in a previous study, we reported low hand stiffness only in the direction perpendicular to the movement during point-to-point two-joint movements constrained in a straight line (Gomi et al. 1992), it was insufficient for predicting an EP trajectory for which full stiffness components are required.

The main purpose of this paper is to formulate a method that allows full components of two-joint arm stiffness (four elements in a stiffness matrix) to be measured during movement. In the proposed method the parameters that depend on arm structure, such as inertia and center of gravity, are estimated independent of posture. Next, we investigate stiffness characteristics during medium speed movements in both transverse and longitudinal directions, and compare them with those during posture maintenance. Furthermore, we will examine whether the EP trajectory of these two kinds of movements estimated from measured impedance parameters is similar to their actual trajectory. A part of this work has been presented in Gomi and Kawato (1996). Note that we do not intend to deny the EP control hypothesis, but rather try to reveal computational requisites for multi-joint arm control.

2 Methods

2.1 Apparatus

Measuring impedance parameters during multi-joint movements is much more difficult than conducting measurements during posture maintenance (Mussa-Ivaldi et al. 1985; Flash and Mussa-Ivaldi 1990; Dolan et al. 1993; Tsuji et al. 1995) or during single-joint movement (Latash and Gottlieb 1991; Bennett et al. 1992; Latash 1992a, b, 1994; 1993). Stiffness measurement invokes application of external forces to the arm by a manipulandum and measurement of the resulting trajectory perturbations. If the perturbation is too strong or the manipulandum is too heavy, subject cannot complete natural movements, and arm stiffness increases to prevent failure. On the other hand, if the perturbation is too small, a reliable estimate cannot be obtained. The manipulandum needs to be (1) fast and light enough to minimize movement interference, while also being (2) strong enough to transmit large forces, and (3) rigid enough to be controlled at high frequencies. It is also necessary to (4) support the human arm on a horizontal plane to be free from the force of gravity and to reduce fatigue. Additionally, (5) nonlinear forces due to manipulandum dynamics should be reduced so as not to disturb the arm movements.

To circumvent these problems, we developed the Parallel Link Drive Air-Magnet Floating Manipulandum (PFM). Figure 1 shows the PFM and the experimental setup for measuring human arm stiffness. The two thin links are driven by two wide links, and the wide links are directly driven by two electric torque motors placed under the metal table. The handle of the manipulandum (subject's hand position) is supported by a friction-free air-magnet floating mechanism that prevents the subject's arm from leaning. Because of this special mechanism and parallel-link structure, no bending force is imposed on the links, and the links can be very light and thin but still rigid enough in the horizontal plane. The handle and the supporting beam can be rotated freely at the top of the links on the horizontal plane. The subject's hand position (handle center) was measured with joint-position sensors (409 600 pulse/rev) of the PFM, and the force exerted on the hand by the PFM was measured by a force sensor (resolution 0.006 kg) placed between the handle and the PFM links. The PFM was controlled by a digital signal processor (0.5 ms/cycle) to reduce the dynamical effects of the PFM on the subject's hand. The minimum mechanical rigidity of PFM at the handle position within the measurement area (0.5×0.8 m) is 32.8×10^3 N/m. The maximum speed, acceleration, and force are 4 m/s, 50 m/s^2, and 150 N, respectively.

2.2 Experiment

2.2.1 Configuration. Three subjects (two males and one female, 26–34 years old, right handed) participated in this study. The subject sat in front of the PFM and was held to the chair-back by straps as shown in Fig. 1. The x-axis indicates the rightward direction and the y-axis indicates the frontal direction away from the body. The origin for both axes is the shoulder position. The right forearm was placed in a molded plastic cuff (0.47 kg) tightly coupled to the handle (the same movements of the handle, the cuff, and the arm were confirmed in advance by an optical position sensor), and supported in the vertical direction by the beam (0.4 kg). A computer monitor was placed behind the PFM to provide targets and current handle position.

2.2.2 Static-stiffness experimental procedure. During static-stiffness measurements, the PFM was controlled to be located at particular positions by a high-gain position servo. Each subject was instructed to relax his or her arm at that position, and was asked to keep zero force vector not to exert external force (Fig. 1). Trapezoidal positional

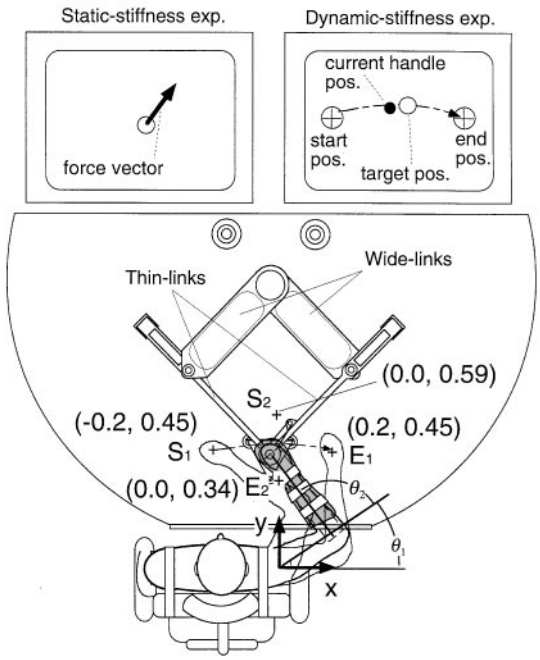

Fig. 1. The Parallel Link Drive Air-Magnet Floating Manipulandum (PFM) system and the experimental setup for measuring human arm stiffness. S_1 and E_1 respectively denote the start and end (positions for the dynamic-stiffness experiments in the transverse movement; S_2 and E_2 are those in the longitudinal movement. The origin of the axes is the shoulder position. The right forearm was covered with a molded plastic cuff, and was tightly fixed to the handle and the beam supporting the forearm in the vertical direction. On the computer monitor during the dynamic-stiffness experiments, the start and end positions, the target marker of the reference trajectory, and current handle position marker were displayed as shown in the *top right* of this figure. During the static-stiffness experiments, force vector in the horizontal plane was displayed on the computer monitor as shown in the *top left* of this figure

perturbations were applied to push the hand and pull it back (6–8 mm) in eight directions within a brief period (about 0.3 s). Forty trials (five trials in each direction, randomly ordered) were recorded in one set for each of five postural conditions (see Results).

2.2.3 Dynamic-stiffness experimental procedure. The subject was instructed to move his or her hand from the start to the end position, both of which were displayed on the computer monitor. The start and end positions were specified as $[x, y] = [-0.2, 0.45]$ (S_1) and [0.2, 0.45] (E_1) m, respectively, in the transverse movement, and as $[x, y] =$ [0, 0.59] (S_2) and [0, 0.34] (E_2) m, respectively, in the longitudinal movement. Movement duration was instructed to be 1 s, indicated by beeping sounds (see also the caption to Fig. 3). To reduce variance, a reference hand trajectory, which itself consisted of each subject's averaged trajectory from 72 pre-trials, was also displayed as target (open circle) movement on the computer monitor. The handle could be moved in any horizontal direction without positional constraint. Small force perturbations for brief periods (about 0.2 s), with nine randomized timings and eight directions, were applied during movement. The subject was also instructed to move his or her hand in as relaxed a way as possible and 'not to intervene voluntarily' (i.e., not to correct his or her movements even if the target was missed because of the perturbation), as in studies by Latash (1992b, 1994). Only those trajectories close to the reference trajectory (< 3 cm at each time step) were recorded for data analysis. In one experiment, eight data sets (72 trials in one set) were recorded without failed trials which deviated more than 3 cm from the reference trajectory except for the perturbation duration.

2.3 Data analysis

Two-link human arm dynamics on the horizontal plane were modeled by the following second-order nonlinear differential equation:

$$\Psi(\ddot{\mathbf{q}}, \dot{\mathbf{q}}, \mathbf{q}) = \boldsymbol{\tau}_{\text{in}}(\dot{\mathbf{q}}, \mathbf{q}, \mathbf{u}) + \boldsymbol{\tau}_{\text{ext}} \tag{1}$$

Here, $\Psi(\cdot)$ denotes a two-link arm dynamics, and $\mathbf{q}$, $\dot{\mathbf{q}}$ and $\ddot{\mathbf{q}}$ are angular position [$\mathbf{q} = (\theta_1, \theta_2)^T$, where θ_1 is shoulder angle and θ_2 is elbow angle], velocity, and acceleration vector, respectively. $\boldsymbol{\tau}_{\text{ext}}$ denotes the external force. Considering the length-tension and velocity-tension relationships of muscle forces, the generated torque, $\boldsymbol{\tau}_{\text{in}}$, can be represented as a function of angular position, velocity, and motor command, $\mathbf{u}$, descending form the supraspinal central nervous system (CNS). To estimate stiffness, viscosity, and inertia parameters by applying small perturbations, the following variational equation can be utilized:

$$\frac{\partial \Psi}{\partial \ddot{\mathbf{q}}}\delta\ddot{\mathbf{q}} + \frac{\partial \Psi}{\partial \dot{\mathbf{q}}}\delta\dot{\mathbf{q}} + \frac{\partial \Psi}{\partial \mathbf{q}}\delta\mathbf{q} = \frac{\partial \boldsymbol{\tau}_{\text{in}}}{\partial \dot{\mathbf{q}}}\delta\dot{\mathbf{q}} + \frac{\partial \boldsymbol{\tau}_{\text{in}}}{\partial \mathbf{q}}\delta\mathbf{q} + \delta\boldsymbol{\tau}_{\text{ext}} \tag{2}$$

If we assume the arm to be rigid body serial link system, such as:

$$\Psi(\ddot{\mathbf{q}}, \dot{\mathbf{q}}, \mathbf{q}) = \mathbf{I}(\mathbf{q})\ddot{\mathbf{q}} + \mathbf{H}(\dot{\mathbf{q}}, \mathbf{q}) \tag{3}$$

and we represent muscle viscosity and stiffness matrix (2×2) as $\mathbf{D}$ and $\mathbf{R}$ such as:

$$-\frac{\partial \boldsymbol{\tau}_{\text{in}}}{\partial \dot{\mathbf{q}}} \equiv \mathbf{D} = \begin{bmatrix} D_{\text{ss}} & D_{\text{se}} \\ D_{\text{es}} & D_{\text{ee}} \end{bmatrix}, \quad -\frac{\partial \boldsymbol{\tau}_{\text{in}}}{\partial \mathbf{q}} \equiv \mathbf{R} = \begin{bmatrix} R_{\text{ss}} & R_{\text{se}} \\ R_{\text{es}} & R_{\text{ee}} \end{bmatrix} \tag{4}$$

then (2) can be written as

$$\mathbf{I}\delta\ddot{\mathbf{q}} + \frac{\partial \mathbf{H}}{\partial \dot{\mathbf{q}}}\delta\dot{\mathbf{q}} + \left(\frac{\partial \mathbf{I}\ddot{\mathbf{q}}}{\partial \mathbf{q}} + \frac{\partial \mathbf{H}}{\partial \mathbf{q}}\right)\delta\mathbf{q} = -\mathbf{D}\delta\dot{\mathbf{q}} - \mathbf{R}\delta\mathbf{q} + \delta\boldsymbol{\tau}_{\text{ext}} \tag{5}$$

Here, $\mathbf{I}$ and $\mathbf{H}$ denote the inertial matrix (2×2) and coriolis-centrifugal force vector respectively, and are represented in (6) and (7). The subscripts 'ss' of D and R represents the shoulder single-joint effect on each coefficient. Similarly, 'se' and 'es' denote double-joint (or interlimb) effects, and 'ee' denotes the elbow single-joint effect.

$$\mathbf{I} = \begin{bmatrix} I_{11} & I_{12} \\ I_{21} & I_{22} \end{bmatrix}$$

$$\begin{aligned} I_{11} &= m_1 l_{g1}^2 + m_2(l_1^2 + l_{g2}^2) + \tilde{I}_1 + \tilde{I}_2 + 2m_2 l_1 l_{g2}\cos\theta_2 \\ &\equiv Z_1 + 2Z_2\cos\theta_2 \end{aligned} \tag{6}$$

$$I_{12} = I_{21} = m_2 l_{g2}^2 + \tilde{I}_2 + m_2 l_1 l_{g2}\cos\theta_2 \equiv Z_3 + Z_2\cos\theta_2$$

$$I_{22} = m_2 l_{g2}^2 + \tilde{I}_2 \equiv Z_3$$

$$\mathbf{H} = \begin{bmatrix} -m_2 l_1 l_{g2}\sin\theta_2(\dot{\theta}_2^2 + 2\dot{\theta}_1\dot{\theta}_2) \\ m_2 l_1 l_{g2}\dot{\theta}_1^2\sin\theta_2 \end{bmatrix} = \begin{bmatrix} -Z_2\sin\theta_2(\dot{\theta}_2^2 + 2\dot{\theta}_1\dot{\theta}_2) \\ Z_2\dot{\theta}_1^2\sin\theta_2 \end{bmatrix} \tag{7}$$

Here, m_1 and m_2 denote the masses of upper arm and forearm links, l_{g1} and l_{g2} denote the length from each joint to the center of gravity for each link, $\tilde{I}_1$ and $\tilde{I}_2$ denote the inertia for each link, and l_1 denotes the length of the upper arm. These parameters can be merged into three parameters Z_1, Z_2, Z_3 (we call these parameters 'structural parameters') as shown in (6) and (7), which are independent of posture. Differentiating $\mathbf{I}$ and $\mathbf{H}$ by $\dot{\mathbf{q}}$ and $\mathbf{q}$, respectively, we obtain:

$$\frac{\partial \mathbf{H}}{\partial \dot{\mathbf{q}}} = \begin{bmatrix} -2Z_2\dot{\theta}_2\sin\theta_2 & -2Z_2(\dot{\theta}_1 + \dot{\theta}_2)\sin\theta_2 \\ 2Z_2\dot{\theta}_1\sin\theta_2 & 0 \end{bmatrix} \tag{8}$$

$$\begin{aligned} \frac{\partial \mathbf{I}\ddot{\mathbf{q}}}{\partial \mathbf{q}} + \frac{\partial \mathbf{H}}{\partial \mathbf{q}} &= \begin{bmatrix} 0 & -Z_2(2\ddot{\theta}_1 + \ddot{\theta}_2)\sin\theta_2 \\ 0 & -Z_2\ddot{\theta}_1\sin\theta_2 \end{bmatrix} \\ &\quad + \begin{bmatrix} 0 & -Z_2(\dot{\theta}_2^2 + 2\dot{\theta}_1\dot{\theta}_2)\cos\theta_2 \\ 0 & -Z_2\dot{\theta}_1^2\cos\theta_2 \end{bmatrix} \end{aligned} \tag{9}$$

Then, (5) can be linearized with respect to the unknown parameters (i.e., structural parameters Z_i, viscosity D_{ij}, and stiffness R_{ij}), as shown in (10):

$$\begin{bmatrix} \zeta_1 & \zeta_2 & \zeta_3 & \zeta_4 & \zeta_5 & \zeta_6 & \zeta_7 & \zeta_8 & \zeta_9 & \zeta_{10} & \zeta_{11} \\ \zeta_{12} & \zeta_{13} & \zeta_{14} & \zeta_{15} & \zeta_{16} & \zeta_{17} & \zeta_{18} & \zeta_{19} & \zeta_{20} & \zeta_{21} & \zeta_{22} \end{bmatrix} \cdot \mathbf{N} = \delta\boldsymbol{\tau}_{\text{ext}} \quad (10)$$

Here, $\mathbf{N}$ is the parameter vector, which can be estimated by the pseudo-inverse method from $\delta\boldsymbol{\tau}_{\text{ext}}$ and ζ_i computed as follows:

$$\delta\boldsymbol{\tau}_{\text{ext}} = [\delta\tau_{\text{ext1}} \;\; \delta\tau_{\text{ext2}}]^T$$

$$\mathbf{N} = [Z_1 \;\; Z_2 \;\; Z_3 \;\; D_{\text{ss}} \;\; D_{\text{se}} \;\; D_{\text{es}} \;\; D_{\text{ee}} \;\; R_{\text{ss}} \;\; R_{\text{se}} \;\; R_{\text{es}} \;\; R_{\text{ee}}]^T$$

$$\zeta_1 = \delta\ddot{\theta}_1, \quad \zeta_3 = \delta\ddot{\theta}_2, \quad \zeta_{14} = \delta\ddot{\theta}_1 + \delta\ddot{\theta}_2,$$

$$\zeta_4 = \zeta_{17} = \delta\dot{\theta}_1, \quad \zeta_5 = \zeta_{18} = \delta\dot{\theta}_2$$

$$\begin{aligned} \zeta_2 = {} & \cos\theta_2(2\delta\ddot{\theta}_1 + \delta\ddot{\theta}_2 - (\dot{\theta}_2^2 + 2\dot{\theta}_1\dot{\theta}_2)\delta\theta_2) \\ & - \sin\theta_2(2\dot{\theta}_2\delta\dot{\theta}_1 + 2(\dot{\theta}_1 + \dot{\theta}_2)\delta\dot{\theta}_2 + (2\ddot{\theta}_1 + \ddot{\theta}_2)\delta\theta_2) \end{aligned} \quad (11)$$

$$\zeta_{13} = \cos\theta_2(\delta\ddot{\theta}_1 + \dot{\theta}_1^2\delta\theta_2) + \sin\theta_2(2\dot{\theta}_1\delta\dot{\theta}_1 - \ddot{\theta}_1\delta\theta_2)$$

$$\zeta_8 = \zeta_{21} = \delta\theta_1, \quad \zeta_9 = \zeta_{22} = \delta\theta_2$$

$$\zeta_6 = \zeta_7 = \zeta_{10} = \zeta_{11} = \zeta_{12} = \zeta_{15} = \zeta_{16} = \zeta_{19} = \zeta_{20} = 0$$

The stability of this estimation method was confirmed by a computer simulation in Gomi and Kawato (1995). In (11), note that Z_1, Z_2, and Z_3 are independent of arm position, velocity, acceleration, and torque, thus indicating that they should be constant values under all conditions. Thus if Z_i can be pre-estimated, we can reduce the number of estimation parameters from 11 to eight in each condition. In other words, the left-hand side of (5) could be calculated by using pre-estimated structural parameters Z_i, and this could be subtracted from $\delta\boldsymbol{\tau}_{\text{ext}}$ in advance to estimate other parameters, D_{ij}, and R_{ij}. In our analysis shown below, Z_i are pre-determined from all data sets.

To use the above method, $\delta\boldsymbol{\tau}_{\text{ext}}$, $\delta\mathbf{q}$, $\delta\dot{\mathbf{q}}$, and $\delta\ddot{\mathbf{q}}$, driven by perturbation, should be extracted from each piece of data that varied in time during movement and that were slightly different from trial to trial. As explained earlier, each perturbation was applied for a short duration and at a given time. At the start of the perturbation, it is reasonable to presuppose from the causality that the offset in position and torque for each trial is due to trial fluctuations, and thus could be canceled out. According to this idea, the following procedure was applied to extract the variational component of position $\delta\mathbf{q}$:

$$\mathbf{q}_{\text{s}}^i(t) = \mathbf{q}^i(t) - \mathbf{q}^i(t_p) \quad (12)$$

$$\mathbf{q}_{\text{s\_av}}(t) = \frac{1}{n}\sum_i^n \mathbf{q}_{\text{s}}^i(t) \quad (13)$$

$$\delta\mathbf{q}^i(t) = \mathbf{q}_{\text{s}}^i(t) - \mathbf{q}_{\text{s\_av}}(t) \quad (14)$$

Here, the superscripts denote the number of the trial, and t_p denotes the start time of the perturbation. $\mathbf{q}_{\text{s}}^i$ denotes the ith trajectory unbiased at the perturbation start. The same procedure was used for velocity, acceleration, and torque data. To eliminate the effect of fluctuation among trials, the data for different trials with the same perturbation were averaged. We used the variational data of the short period after the perturbation commenced ($t_p \leqslant t \leqslant t_p + t_{\text{est}}$; for the static condition $t_{\text{est}} = 0.4$ s; for the dynamic condition $t_{\text{est}} = 0.28$ s) for the parameter estimation described above.

3 Results

3.1 Estimated structural parameters

As explained above, because the structural parameters, Z_i, are independent of posture and movement, their values can be fixed in any posture for each subject. This reduces estimation errors caused by partially correlated data under some conditions. To fix the structural parameters, we first estimated all 11 parameters in $\mathbf{N}$ (11) using all data sets obtained under many different conditions. The performance indexes, *coefficients of determination* (Hines and Montgomery 1972), for the reconstructed variational torques ($\delta\boldsymbol{\tau}_{\text{ext}}$) were 0.984 ± 0.004 (mean $\pm$ SD) for all subjects under the static conditions and 0.945 ± 0.042 for all subjects under the dynamic conditions. The structural parameters obtained for each subject are summarized in Table 1. Note that all values should be greater than those of the subject's inherent arm dynamics, because they include entities of the plastic cuff, the supporting beam, and the handle.

3.2 Stiffness during posture maintenance

Figure 2 shows the stiffness ellipses (upper row) and joint-stiffness values (lower row) for three subjects during posture maintenance at five positions. The coefficient of determination for reconstructed variational torque depending only on stiffness and viscosity (i.e., $\mathbf{D}\delta\dot{\mathbf{q}} + \mathbf{R}\delta\mathbf{q}$) had a mean value of 0.855. The hand stiffness matrix, $\mathbf{K}$, for depicting ellipses was obtained from joint stiffness matrix $\mathbf{R}$ using the following equation:

$$\mathbf{K} = (\mathbf{J}^T)^{-1}\left(\mathbf{R} + \frac{\partial\mathbf{J}^T}{\partial\mathbf{q}}\mathbf{F}_{\text{in}}\right)\mathbf{J}^{-1} \quad (15)$$

Here, $\mathbf{F}_{\text{in}}$ denotes force generated by the arm in Cartesian coordinate ($\mathbf{J}^T\tau_{\text{in}}$), and $\mathbf{J}$ denotes the Jacobian matrix of kinematic transformation. Note that the internal force, $\mathbf{F}_{\text{in}}$, is zero under the static condition without external force. Each stiffness ellipse represents the direction and magnitude of elastic, resisting forces to unit-length positional perturbations in all directions. The major axis of each ellipse represents the maximum force, which indicates the greatest stiffness. Conversely, the minor axis represents the minimum force, indicating the least stiffness. As shown in the upper rows of Fig. 2, the orientations and shapes of the stiffness ellipses were similar for all subjects in each corresponding posture, and the major axes of stiffness ellipses in all postures were directed to the shoulder as previously studied (Mussa-Ivaldi et al. 1985; Flash and Mussa-Ivaldi 1990; Dolan et al. 1993; Tsuji et al. 1995). The magnitude of stiffness (represented here as the area of the ellipse) for subject B (female) was less than for subjects A and C (males). The ellipse sizes in our experiment were several times smaller than those in the experiments by Mussa-Ivaldi et al. (1985) and Flash

Table 1. The structural parameters estimated from all data for each subject

Subject	Z_1 N m/(rad/s^2)	Z_2 N m/(rad/s^2)	Z_3 N m/(rad/s^2)
A	0.451	0.158	0.153
B	0.318	0.100	0.104
C	0.403	0.166	0.140

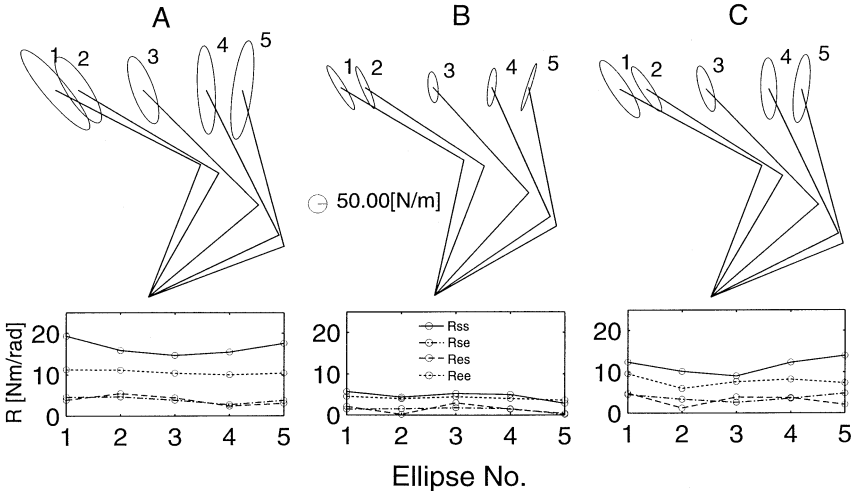

Fig. 2. Stiffness ellipses (*upper figures*) and joint stiffness values (*lower figures*) during posture maintenance of subjects *A*, *B*, and *C*. During the experiments, the subjects were asked to relax and not to exert any force against PFM, assisted by visual feedback of a force vector on the computer monitor (see Fig. 1 and Static-stiffness experimental procedure in the text). The visual feedback was frozen during perturbation

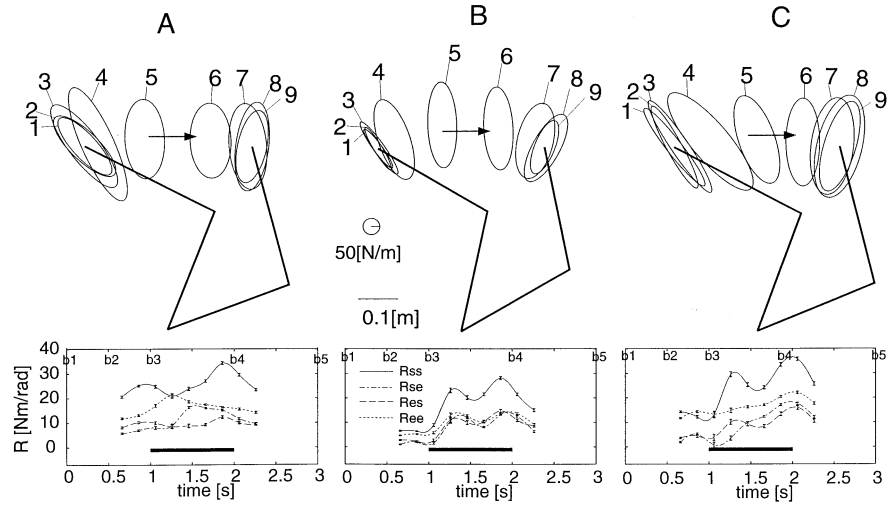

Fig. 3. Stiffness ellipses (*upper figures*) and joint stiffness values (*lower figures*) of shoulder (R_{ss}, *continuous curve*), elbow (R_{ee}, *dotted curve*), and double-joints (R_{se}, *dashed-dotted curve*: R_{es}, *dashed curve*) during transverse multi-joint movements (see Dynamic-stiffness experimental procedure in the text) for subjects *A*, *B* and *C*. In the *upper figures*, the starting and ending arm configurations are shown as *thick sticks*. The center of each stiffness ellipse is located at the hand position for the corresponding arm configuration during the movement. Time 0 in the *lower figures* denotes the first beep sound (*b1*). Subjects were instructed to start from position S_1 (Fig. 1) at the third beep (*b3*), to stop at position E_2 at the fourth beep (*b4*), and to hold their hand there until the fifth beep (*b5*). As shown above the abscissa of the lower figures, b2, b3, b4 and b5 were given 0.5, 1.0, 2.0 and 3.0 s after b1. The *thick horizontal line* denotes the instructed movement duration. The perturbation force used for measuring stiffness of the third ellipse began 0.1 s before b3 (movement start), and that for the eight ellipse began 0.1 s before b4 (movement end)

and Mussa-Ivaldi (1990), and were comparable to those of Tsuji et al. (1995). This difference might be due to the different instructions in their experiments for gripping force, which change muscle activations at the elbow and shoulder as presented in Tsuji et al. (1995).

As shown in the lower row of Fig. 2, shoulder-joint stiffness values (R_{ss}) were higher than elbow-joint stiffness values (R_{ee}) for all postures and all subjects. Double-joint stiffness values (R_{se}, R_{es}) at each posture were almost the same as each other. The ratios between the double-joint stiffness values (R_{se}, R_{es}) and the single-joint stiffness values (R_{ss}, R_{ee}) were about 1:2.5–4.5, suggesting that double-joint muscles were weakly activated compared with the single-joint muscles under this experimental condition.

3.3 Stiffness during point-to-point movement

The upper row of Fig. 3 shows stiffness ellipses for three subjects during multi-joint movement in a transversal direction. The coefficient of determination for reconstructed variational torque depending only on $\mathbf{D}\delta\dot{\mathbf{q}} + \mathbf{R}\delta\mathbf{q}$ had a mean value of 0.806. Because 0.28 s of data were used to estimate stiffness after the perturbation was initiated, both the intrinsic elastic properties of the muscles and reflexes contributed to the estimated

stiffness. The numbers attached to these ellipses indicate nine specified moments, each separated by 0.2 s, before the movement (1 and 2), at the start of the movement (3), during the movement (4 to 7) and after (8 and 9) the movement. At the first perturbation, the stiffness ellipses were thin with their major axes oriented toward the shoulder, which is a common feature of stiffness ellipses during posture maintenance, as noted above. The ellipse began to enlarge around the commencement of movement (2 to 4). The areas of the ellipses during movement (4 to 7) were on average 7.2 times greater than those during relaxed, corresponding postures. This increase most likely reflects the muscle tension required to execute the movement. Along with the change in size, the shape of the ellipses during movement (4 to 7) thickened slightly in comparison with those while posture was maintained (ratio of major and minor axes: movement 2.7 ± 0.6, posture 5.1 ± 2.3).

The lower row of Fig. 3 shows the temporal changes in shoulder, elbow, and double-joint stiffness during movement with their 90% double-sided confidence intervals. Shoulder stiffness increased around the commencement of the movement, decreased slightly in the middle of the movement, then increased again around the end of the movement. This observation is similar to that of the elbow single-joint movement (Bennett 1993). The timing of the stiffness decrease may be due to switch from shoulder extensor activation to shoulder flexor activation, because shoulder extension is the dominant component in the movements examined. The ratio of stiffness components for shoulder, elbow, and double-joints changed dynamically, indicating that muscle activities changed greatly during movement. Note that, although ratios of stiffness components altered during movement, the double-joint stiffness values (R_{se}, R_{es}) during movement were lower than the elbow joint stiffness (R_{ee}). In contrast with single-joint cyclic movement (Bennett et al. 1992), the joint stiffness values during multi-joint movement were always greater than those during corresponding postures. All stiffness components decreased after the movement ceased although stiffness had not yet been restored to static stiffness. Present results (range 5–21 N m/rad) do not differ greatly from the elbow-joint stiffness (range 3–14 N m/rad) during single-joint movement explored by different perturbation patterns (random and step at several amplitudes) (Bennett et al. 1992; Bennett 1993). The slightly greater stiffness in the observed multi-joint movement might be ascribed to the effects of interactional forces between the upper arm and the forearm. The double-joint stiffness components (R_{se}, R_{es}) were sometimes asymmetric during movement in subjects A and C as previously observed in a catching task (Lacquaniti et al. 1993). Double-joint stiffness ascribed to the inherent mechanical property of muscle should be intrinsically symmetric; thus our observation suggests that the reflex contribution during movement is different from that under static conditions.

Figure 4 shows the stiffness ellipses and the temporal changes in joint stiffness values during multi-joint movement in the longitudinal direction for subjects A and C.

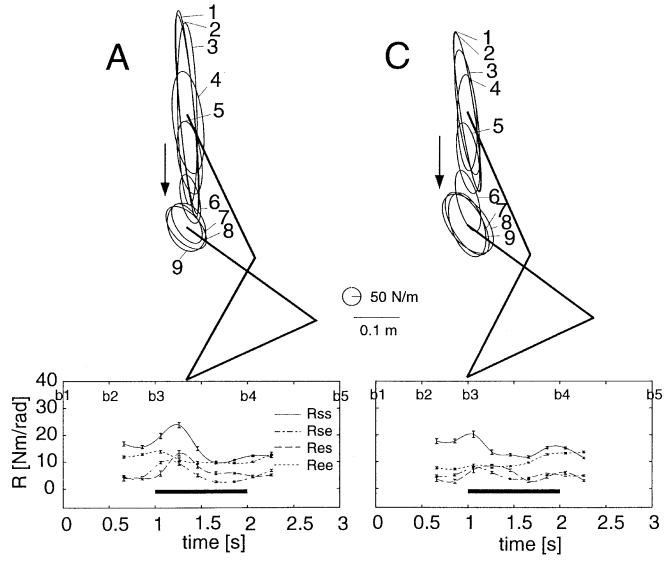

Fig. 4. Stiffness ellipses (*upper figures*) and joint stiffness values (*lower figures*) of shoulder (R_{ss}, *continuous curve*), elbow (R_{ee}, *dotted curve*), and double-joints (R_{se}, *dashed-dotted curve*; R_{es}, *dashed curve*) during the longitudinal multi-joint movements for subjects *A* and *C*. All *notation* is as in Fig. 3

The coefficient of determination for reconstructed variational torque depending only on $\mathbf{D}\delta\dot{\mathbf{q}} + \mathbf{R}\delta\mathbf{q}$ had a mean value of 0.799. For subject B, the experimental setup could not be applied because the posture at the start position was close to subject's workspace boundary (i.e., singular condition). The stiffness ellipses were thin near the start position, and were wide near the end position. The temporal changes in ellipse shapes for subjects A and C were similar, and not very different from those during static conditions (not shown here).

The shoulder-joint stiffness components of both subjects, shown in the lower row of Fig. 4, increased in the initial phases of the longitudinal movements as in those of the transverse movements, but not in the final phases of the longitudinal movements. This difference was ascribed to differences in posture at the end position and the movement speeds of two different movements. The decelerating torque near the end position of the longitudinal movement was not much required (peak deceleration shoulder torque 0.53 N m on average for subjects A and C) compared with that in the transverse movement (peak deceleration torque 2.19 N m on average for subjects A and C).

3.4 Predicted EP trajectory during free movements

The measured dynamic stiffness allowed us to predict the EP trajectory, which has been proposed as a potential motor command from the CNS in voluntary movement (Bizzi et al. 1984, 1992; Hogan 1984; Feldman 1986). According to the α-version of the EP hypothesis (Bizzi et al. 1984; Hogan 1984), the $\boldsymbol{\tau}_{in}$ is represented by the following equation:

$$\boldsymbol{\tau}_{in} = \mathbf{R}(\mathbf{q}_{eq} - \mathbf{q}) - \mathbf{D}\dot{\mathbf{q}} \tag{16}$$

Here, $\mathbf{q}_{eq}$ denotes the equilibrium position represented in joint-angle coordinates. This equation is derived from the linear approximation of $\boldsymbol{\tau}_{in}$ in (1) around the actual trajectory as in (2) and (5). Note that $\boldsymbol{\tau}_{in} = 0$ holds while $\mathbf{q} = \mathbf{q}_{eq}$, $\dot{\mathbf{q}} = 0$ from the definition of equilibrium position. The equilibrium position in joint coordinate $\mathbf{q}_{eq}$ and in Cartesian coordinate x_{eq} are derived as follows:

$$\mathbf{q}_{eq} = \mathbf{R}^{-1}(\mathbf{I}\ddot{\mathbf{q}} + \mathbf{H}(\dot{\mathbf{q}}, \mathbf{q}) + \mathbf{D}\dot{\mathbf{q}} - \boldsymbol{\tau}_{ext}) + \mathbf{q}, \quad x_{eq} = \Phi(\mathbf{q}_{eq}) \tag{17}$$

Here, $\mathbf{q}$, $\dot{\mathbf{q}}$ and $\ddot{\mathbf{q}}$ are the actual trajectory (unperturbed), its velocity, and its acceleration, respectively. $\boldsymbol{\tau}_{ext}$ denotes torque measured by the force sensor. By using the structural parameters Z_i (in **I** and **H**), **R**, and **D** previously estimated, the EP trajectory can be calculated from the experimental data. This linearized method could be criticized because of the nonlinear relationship between length and tension of muscle; however, the global behavior of a single joint has been roughly approximated by a linear relationship in both the flexion and extension directions (Zeffiro 1986; Gottlieb and Agarwal 1988). The effect of the linearization error will be discussed below.

Figure 5 shows spatial paths (top row), the position along the main movement direction (x-axis for Fig. 5a and y-axis for Fig. 5b) as a function of movement time (middle row), and tangential velocity profiles (bottom row) of actual (dashed line) and equilibrium (continuous line) trajectories predicted by using smoothly interpolated impedance parameters. The maximum errors in predicting equilibrium positions calculated from 90% confidence intervals of the estimated stiffness and viscosity were 0.005 ± 0.0063 m and 0.0009 ± 0.001 (mean $\pm$ SD) respectively in the transverse and longitudinal movements for nine positions and three subjects, indicating high reliability of the estimate (individual data are shown as error bars in Fig. 5, middle row). The spatial paths of equilibriums (continuous lines in the top row) did not deviate much from the actual paths (dashed line). However, as shown in the middle row of Fig. 5, the equilibrium position first led the actual position to generate the accelerating torque, then fell behind the actual position to generate the decelerating torque. As a result of these differences, all the velocity profiles of the EP trajectory had multiple peaks which are very different from the actual ones. The EP velocity, in particular, increased rapidly and peaked just after the initiation of the movement. This indicates that dynamic stiffness is not sufficiently high to maintain the equilibrium close to the actual position, and that dynamical effects need to be taken into account in movement execution, even if the motor command is an EP trajectory.

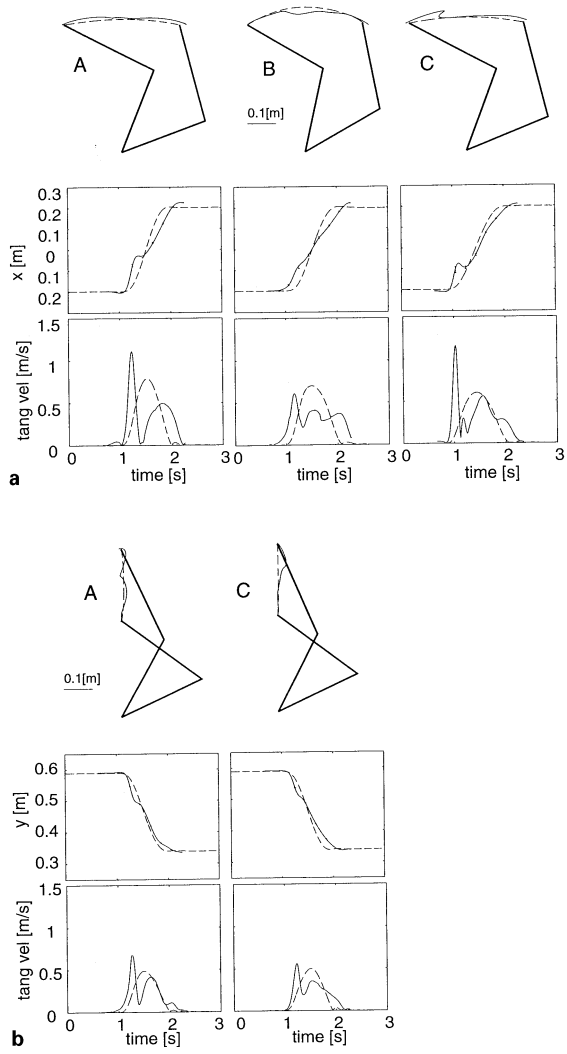

Fig. 5a, b. The spatial paths (*top figures*), position along a line parallel to the x-axis (**a**) or y-axis (**b**) (main movement component) as a function of movement time with their error bars calculated from 90% confidence intervals (*middle figures*), and the tangential velocity profiles of the actual (*dashed curves*) and equilibrium-point (*continuous curves*) trajectories (*bottom figures*) for subjects *A*, *B*, and *C*. The model for deriving the equilibrium-point trajectory was described in the text. It was computed every 0.05 s from **R** and **D**, which were interpolated between estimated values at every 0.2 s by an upsampling method. The equilibrium hand position in the Cartesian coordinate was transformed from that in the joint coordinates [see (17)]

4 Discussion

4.1 Underestimated distance between actual and equilibrium positions

Due to the muscle's inherent nonlinear property in the length-tension curve in particular the exponential increase and accelerating nonlinearity (Feldman 1966, 1986; St-Onge et al. 1993; Feldman and Levin 1995)], one could make the criticism that the arm stiffness measured here was underestimated to predict the EP trajectory, resulting in an overestimation of the distance between actual and equilibrium positions. This distance, however, might be estimated to be shorter than it actually was as briefly explained in Gomi and Kawato (1996). Figure 6 depicts an angle-torque relationship of a single joint produced by agonist and antagonist muscles. Stiffness R measured in our experiment denotes the slope of the tangential line around the actual position θ, not around the equilibrium position θ_{eq}^{real}. Considering the

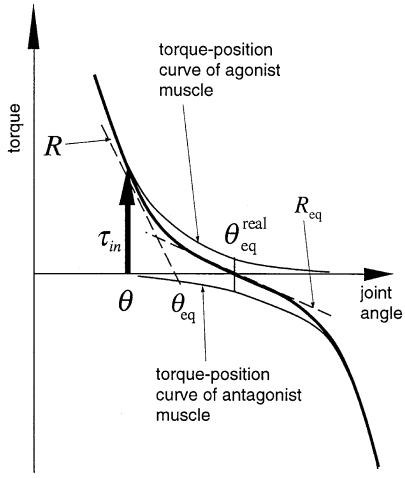

Fig. 6. Angle-torque relationship (*thick curve*) of a single joint produced by agonist and antagonist muscles. θ, θ_{eq}, and θ_{eq}^{real} denote actual, estimated, and real equilibrium positions, respectively. R and R_{eq} denote stiffness values, which are slopes of tangential lines around the actual position (θ) and around the real equilibrium position (θ_{eq}^{real}), respectively. The *thick arrow* represents the generated torque due only to the elasticity

accelerating nonlinear relationship between angle and torque, the measured stiffness $R \equiv \partial\tau_{in}(\theta)/\partial\theta$ is greater than the stiffness around the equilibrium position $R_{eq} \equiv -\partial\tau_{in}(\theta_{eq})/\partial\theta_{eq}$. Thus, as shown in Fig. 6, the equilibrium position θ_{eq} predicted linearly from the measured stiffness R and the actual position θ is always closer to the actual position than the real equilibrium position θ_{qe}^{real}. This can be represented by $|\tau_{in}/R| < |\theta_{eq}^{real} - \theta|$, with the result that the distance between the equilibrium position and the actual position may rather be underestimated in our analyses. Consequently, our main conclusion safely holds while considering the nonlinear property of the musculoskeletal system.

Moreover, because of the task instruction to reduce trajectory errors in our experiments, the stiffness might be increased compared with natural relaxed movements. This might suggest that the equilibrium trajectory was closer to the actual trajectory in this experiment than in natural point-to-point movements. Under non-experimental conditions the stiffness would decrease, and then equilibrium and actual trajectories could deviate greatly, especially in fast movements.

Won and Hogan (1995) conducted experiments and developed an analysis which seemed to indicate that the equilibrium point was close to the actual point in slow movements (16 cm/750 ms). Their experiment demonstrated that the variational force vectors, observed while a trajectory was slightly perturbed in a direction perpendicular to the movement by a circular constraint, were always directed toward the unperturbed realized trajectory. On the basis of these results they asserted that the equilibrium point (or attractor point) remained in the vicinity of the realized trajectory. In the slow and small movements that they studied, however, the equilibrium point should not deviate from the actual point because it is not required to produce large driving torques. For a subject to move his or her hand for long distance at faster speeds, larger torque should be required. Our results indicate that stiffness increases were insufficient to keep the equilibrium point close to the actual one. Additionally, the spatial patterns of equilibrium paths did not deviate greatly from actual trajectories as shown in the top row of Fig. 5, even though the temporal patterns and their velocity profiles (middle and bottom rows of Fig. 5) were quite different from the actual ones. From these considerations, the experimental result by Won and Hogan (1995) does not provide counterevidence to our conclusion that the EP trajectory differs from the actual trajectory during multi-joint fast and large movements.

4.2 Feedforward control by an internal model acquired in the CNS

As discussed above, the experimental data obtained in this study do not support the hypothesis that the brain is not required to conduct complex inverse dynamics computations because of the spring-like properties of muscles and reflex loops. Instead, the data indicate that the dynamics of a controlled object should be accounted for in commanding movements, as suggested from the single-joint experiments (Latash 1994; Gottlieb 1996). As asserted by Bizzi et al. (1992) and Feldman and Levin (1995), we believe that the inherent spring-like properties are beneficial not only in controlling posture, but also in reducing the complexities involved in controlling novel multi-joint movements. Especially in the early stage of movement learning, we suppose that stiffness would be strategically increased to avoid disturbances caused by dynamic interaction forces which still can not be compensated by a poor internal model. This strategy may well correspond to the EP control, as simulated in Flash (1987). Unskilled movements, however, would still be clumsy and would easily be exhausting. As acquisition of knowledge as to how to regulate many muscles for the required movements proceeds, the fatigueless movement with low stiffness could become progressively dominant. From the computational point of view, this knowledge corresponds to an internal model of the controlled object. As the brain acquires internal models of the controlled object, excessive stiffness can be avoided, and mechanical properties of the musculoskeletal system could be optimally regulated according to environmental constraints and the desired tasks. For smooth eye movements, the analyses of Shidara et al. (1993) and Gomi et al. (1994) suggest that the cerebellum sends the motor command based on an internal model of the eye-ball dynamics. On the other hand, many phenomena suggesting that the cerebellum regulates stiffness rather than force or torque were reviewed by Smith (1996). In addition to the computational scheme of internal model learning (Kawato et al. 1987; Gomi and Kawato 1992; Kawato and Gomi 1992), further investigations on the representations of internal models and on the mechanisms regulating stiffness are necessary to reveal biological skillful motor control.

Acknowledgements. We thank M. Honda, K. Ishii of NTT and Y. Tohkura of ATR for their continuing encouragement; G. Gottlieb and S. Schaal for improving the manuscript; N. Imamura, H. Nagaoka of KOBELCO and T. Yoshioka of CSK for their technical support. This work was supported by Human Frontier Science Program grants to M.K.

References

Abend W, Bizzi E, Morasso P (1982) Human arm trajectory formation. Brain 105:311–348

Bennett DJ (1993) Torques generated at the human elbow joint in response to constant position errors imposed during voluntary movements. Exp Brain Res 95:488–498

Bennett DJ, Hollerbach JM, Xu Y, Hunter W (1992) Time-varying stiffness of human elbow joint during cyclic voluntary movement. Exp Brain Res 88:433–442

Bizzi E, Accornero N, Chapple W, Hogan N (1984) Posture control and trajectory formation during arm movement. J Neurosci 4: 2738–2744

Bizzi E, Hogan N, Mussa-Ivaldi FA, Giszter S (1992) Does the nervous system use equilibrium-point control to guide single and multiple joint movements? Behav Brain Sci 15:603–613

Carew TJ (1985) The control of reflex action. In: Kandel ER, Schwartz JH (eds) Principles of neural science. Elsevier, New York, pp 457–468

Carew TJ, Ghez C (1985) Muscles and muscle receptors. In: Kandel ER, Schwartz JH (eds) Principles of neural science. Elsevier, New York, pp 443–456

Dolan JM, Friedman MB, Nagurka ML (1993) Dynamic and loaded impedance components in the maintenance of human arm posture. IEEE Trans Syst Man Cybern 23:698–709

Feldman AG (1996) Functional tuning of nervous system with control of movement or maintenance of a steady posture. II. Controllable parameters of the muscles. Biophysics 11:565–578

Feldman AG (1986) Once more on the equilibrium-point hypothesis (lambda-model) for motor control. J Mot Behav 18:17–54

Feldman AG, Levin MF (1995) The origin and use of positional frames of reference in motor control. Behav Brain Sci 18:723–806

Flanagan JR, Ostry DJ, Feldman AG (1993) Control of trajectory modifications in target-directed reaching. J Mot Behav 25: 140–152

Flash T (1987) The control of hand equilibrium trajectories in multi-joint arm movements. Biol Cybern 57:257–274

Flash T, Hogan N (1985) The coordination of arm movements: an experimentally confirmed mathematical model. J Neurosci 5:1688–1703

Flash T, Mussa-Ivaldi FA (1990) Human arm stiffness characteristics during the maintenance of posture. Exp Brain Res 82:315–326

Gomi H, Kawato M (1992) Adaptive feedback control models of the vestibulocerebellum and spinocerebellum. Biol Cybern 68:105–114

Gomi H, Kawato M (1995) Mechanical impedance of human arm during multi-joint movement in horizontal plane (in Japanese). (Technical Report No. ISRL-95-2) NTT Basic Research Laboratoriès, Atsugi

Gomi H, Kawato M (1966) Equilibrium-point control hypothesis examined by measured arm-stiffness during multi-joint movement. Science 272:117–120

Gomi H, Koike Y, Kawato M (1992) Human hand stiffness during discrete point-to-point multi-joint movement. In: Morucci P, Plonsey R, Coatrieux JL, Laxminarayan S (ed) Proceedings of the 14th annual international conference of the IEEE Engineering in Medicine and Biology Society, vol 4. Paris, pp 1628–1629

Gomi H, Shidara M, Takemura A, Inoue Y, Kawano K, Kawato M (1994) Using an inverse dynamics representation to reconstruct temporal firing patterns of Purkinje-cells in monkey ventral praflocculus. (Technical report no. TR-H-086) ATR Human Information Processing Research Laboratories Soraku-gun

Gottlieb GL (1996) Shifting frames of reference but the same old point of view. Behav Brain Sci 18:758–759

Gottlieb GL, Agarwal GC (1988) Compliance of single joints: elastic and plastic characteristics. Neurophysiol 59:937–951

Hines WW, Montgomery DC (1972) Probability and statistics in engineering and management science, 3rd edn. Wiley, New York

Hogan N (1984) An organizing principle for a class of voluntary movements. Neurosci 4:2745–2754

Katayama M, Kawato M (1993) Virtual trajectory and stiffness ellipse during multi-joint movement predicted by neural inverse models. Biol Cybern 69:353–362

Kawato M, Gomi H (1992) The cerebellum and VOR/OKR learning models. Trends Neurosci 15:445–453

Kawato M, Furukawa K, Suzuki R (1987) A hierarchical neural-network model for control and learning of voluntary movement. Biol Cybern 57:169–185

Kelso JA, Southard DL, Goodman D (1979) On the nature of human interlimb coordination. Science 203:1029–1031

Lacquaniti F, Carrozzo M, Borghese NA (1993) Time-varying mechanical behavior of multijointed arm in man. J Neurophysiol 69:1443–1464

Latash ML (1992a) Independent control of joint stiffness in the framework of the equilibrium-point hypothesis. Biol Cybern 67:377–384

Latash ML (1992b) Virtual trajectories, joint stiffness, and changes in the limb natural frequency during single-joint oscillatory movements. Neuroscience 49:209–220

Latash ML (1994) Reconstruction of equilibrium trajectories and joint stiffness patterns during single-joint voluntary movements under different instructions. Biol Cybern 71:441–450

Latash ML, Gottlieb GL (1991) Reconstruction of shifting elbow joint compliant characteristics during fast and slow movements. Neuroscience 43:697–712

McIntyre J, Bizzi E (1993) Servo hypotheses for the biological control of movement. J Mot Behav 25:193–202

Morasso P (1981) Spatial control of arm movements. Exp Brain Res 42:223–227

Mussa-Ivaldi FA, Hogan N, Bizzi E (1985) Neural, mechanical, and geometric factors subserving arm posture in humans. J Neurosci 5:2732–2743

Shidara M, Kawano K, Gomi H, Kawato M (1993) Inverse dynamics model eye movement control by Purkinje cells in the cerebellum. Nature 365:50–52

Smith AM (1996) Does the cerebellum learn strategies for the optimal time-varying control of joint stiffness? Behav Brain Sci 19

St-Onge N, Qi H, Feldman AG (1993) The patterns of control signals underlying elbow joint movements in humans. Neurosci Lett 164:171–174

Tsuji T, Morasso PG, Goto K, Ito K (1995) Human hand impedance characteristics during maintained posture. Biol Cybern 72:475–485

Won J, Hogan N (1995) Stability properties of human reaching movements. Exp Brain Res 107:125–136

Zeffiro TA (1986) Motor adaptations to alterations in limb mechanisms. PhD Thesis, MIT